Electronic supplementary information

Efficient CO_2 reduction over a Ru-pincer complex/TiO_2 hybrid photocatalyst *via* direct Z-scheme mechanism

Shengtao Chen,‡ Kan Li,‡ Haoran Liu, Jing Zhang* and Tianyou Peng*

College of Chemistry and Molecular Sciences, Engineering Research Center of Organosilicon Compounds & Materials, Wuhan University, Wuhan 430072, China

‡ These authors contributed to this work equally.

* Corresponding authors.

E-mail address: typeng@whu.edu.cn (T. Peng). jzhang03@whu.edu.cn (J. Zhang)

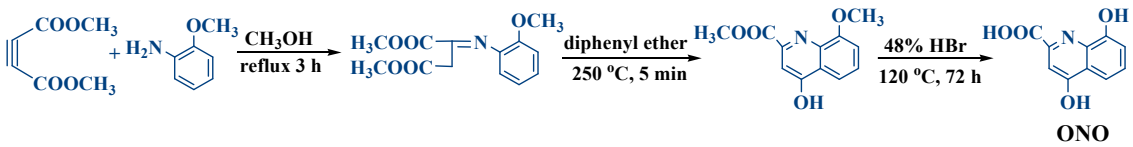

Scheme S1 Synthesis procedure of the ligand ONO (4,8-dihydroxyquinoline-2-carboxylic acid).

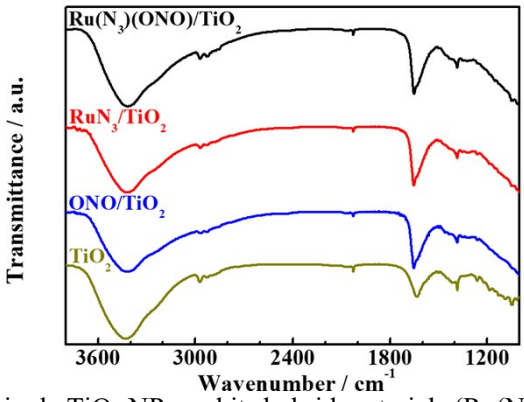

Fig. S1 FTIR spectra of the single TiO_2 NPs and its hybrid materials ($Ru(N_3)(ONO)/TiO_2$, RuN_3/TiO_2 and ONO/TiO_2) with 0.25wt% loading amount.

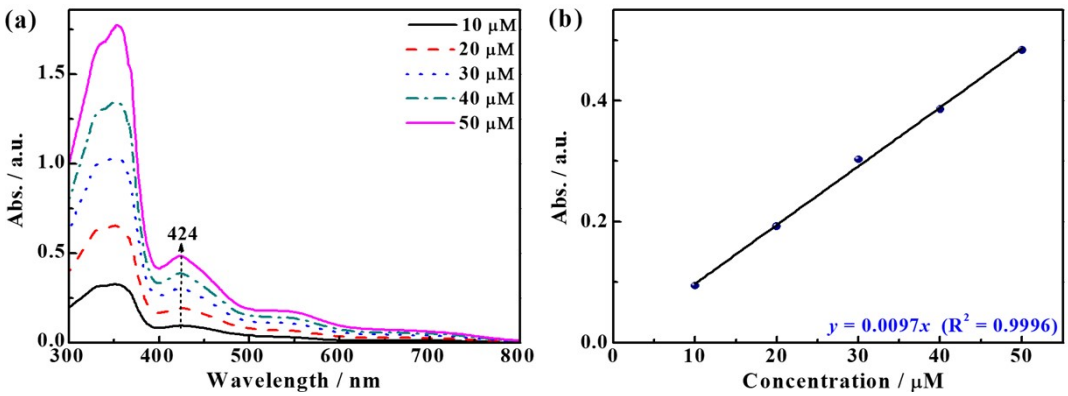

Fig. S2 UV-Vis absorption spectra and calibration curve of the $Ru(N_3)(ONO)$ in DMF solutions with different concentrations.

Table S1 Actual $Ru(N_3)(ONO)$-loading amount of the hybrid materials with different additive amounts

Additive amount / wt%	0	0.05	0.13	0.25	0.50	0.10
Actual amount / wt%	0	0.04	0.10	0.20	0.37	0.71

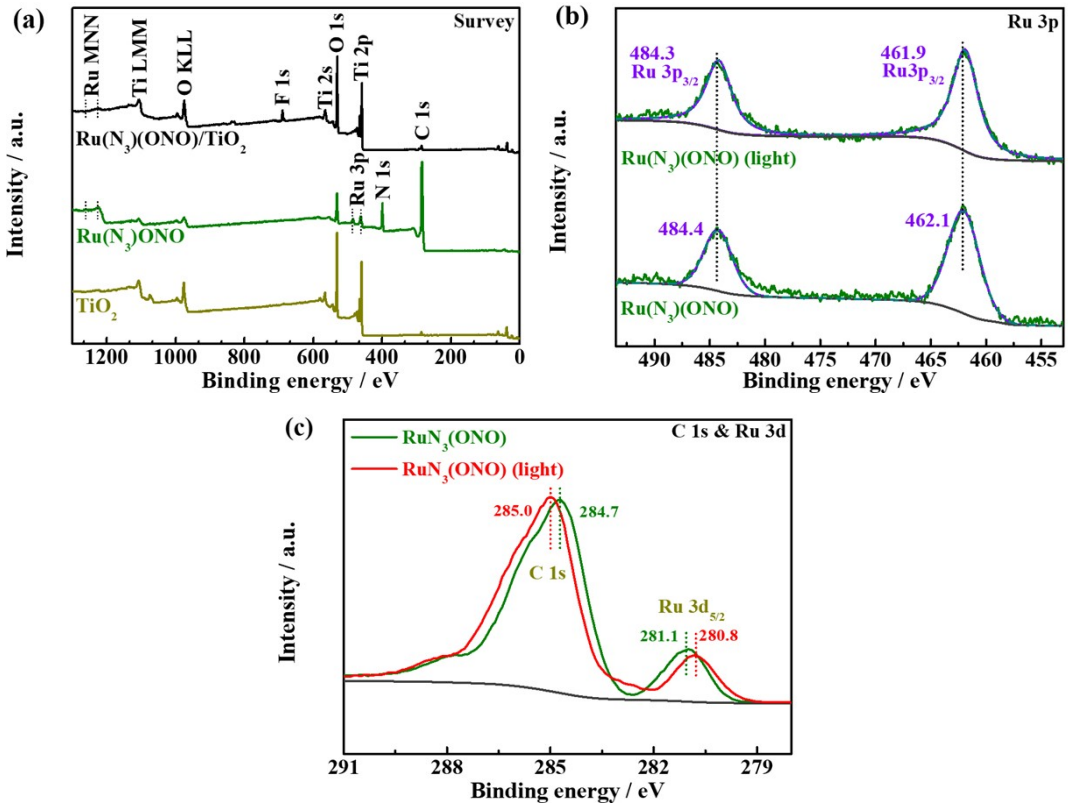

Fig. S3 (a) Survey XPS spectra of the TiO_2 NPs, $Ru(N_3)(ONO)$ complex and 0.25wt% $Ru(N_3)(ONO)/TiO_2$. High-resolution Ru 3p (b) or C 1s & Ru 3d (c) XPS spectrum of the $Ru(N_3)(ONO)$ complex in dark or under 300 W Xe-lamp illumination for 15 min.

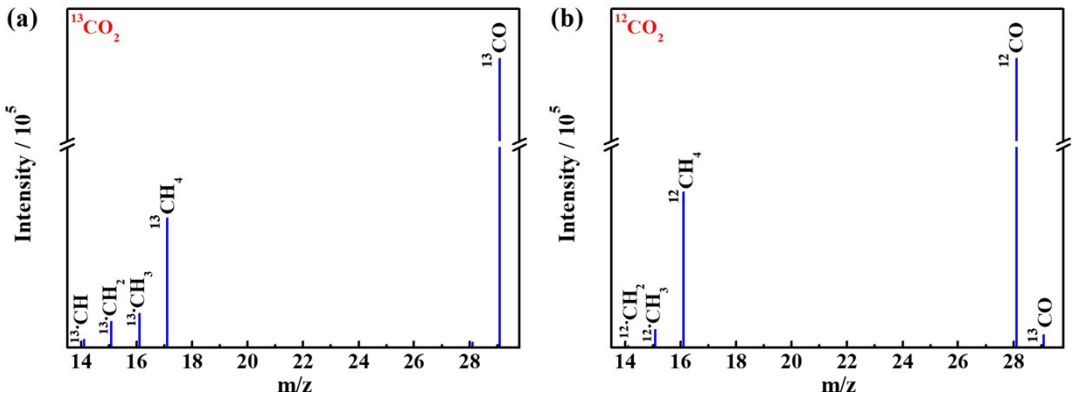

Fig. S4 GC-MS chromatograms of CO/CH_4 produced from the photocatalytic CO_2RR system containing $Ru(N_3)(ONO)/TiO_2$ hybrid material and $^{13}CO_2$ (a) or $^{12}CO_2$ (b) gas as the carbon source.

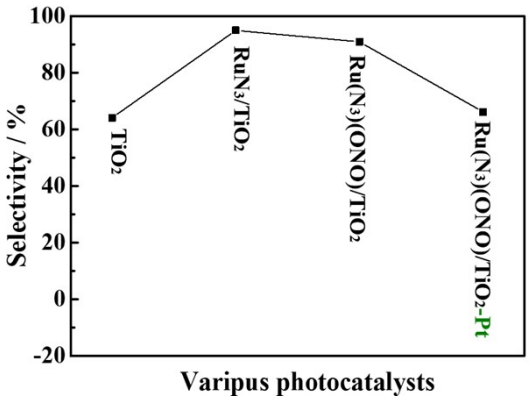

Fig. S5 CO selectivity of TiO_2 NPs, 0.25wt% hybrid materials and Pt loaded ($Ru(N_3)(ONO)/TiO_2$).

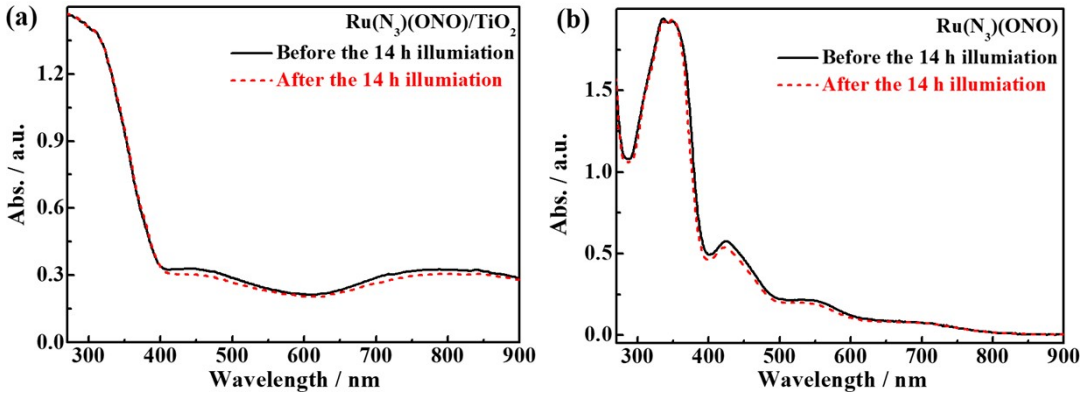

Fig. S6 (a) DRS spectra of the $Ru(N_3)(ONO)/TiO_2$ before/after the photoreaction. (b) UV-Vis spectra of the $Ru(N_3)(ONO)$ in DMF solutions desorbed from the $Ru(N_3)(ONO)/TiO_2$ before/after the photoreaction.

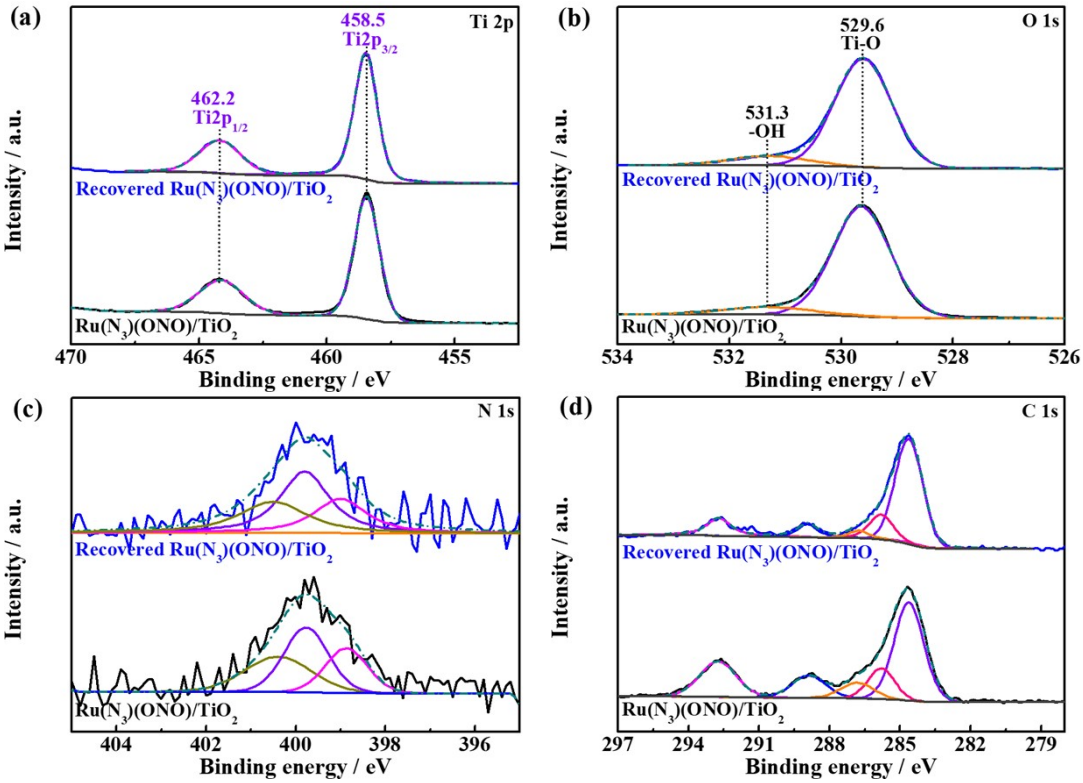

Fig. S7 High-resolution Ti 2p (a), O 1s (b), N 1s (c) and C 1s (d) XPS spectra of the $Ru(N_3)(ONO)/TiO_2$ before and after the 12 h photoreaction.

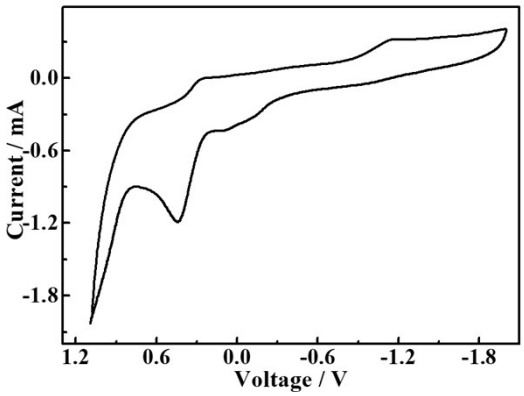

Fig. S8 Cyclic voltammogram of the Ru(N_3)(ONO) complex in DMF solution at room temperature.

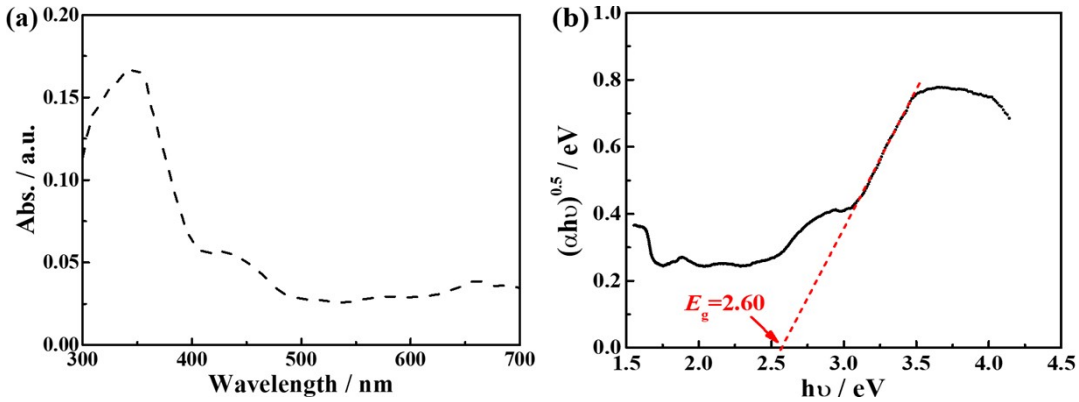

Fig. S9 UV-Vis DRS spectrum (a) and its Tauc plot (b) of the (Ru(N_3)(ONO) complex.

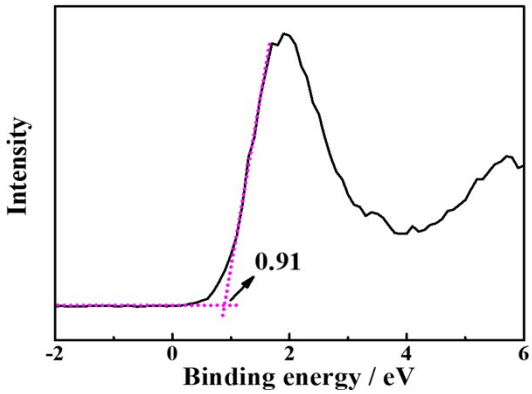

Fig. S10 VB XPS spectrum of the (Ru(N_3)(ONO) complex.

Table S2 Electrochemical data of the Ru(N_3)(ONO) complex

Complex	E_{ox} / V *vs.* SCE	E_{red} / V *vs.* SCE	E_{0-0} / eV	HOMO[a] / V *vs.* NHE	LUMO[b] / V *vs.* NHE
Ru(II) complex	0.78 (Oxd_1)	−0.62 (Red_1)	2.59	0.99	-1.60

[a] Calculated with $E_{HOMO} = -(E_{ox} + 4.71)$ eV. [b] Calculated with $E_{LUMO} = (E_{HOMO} + E_{0-0})$ eV.

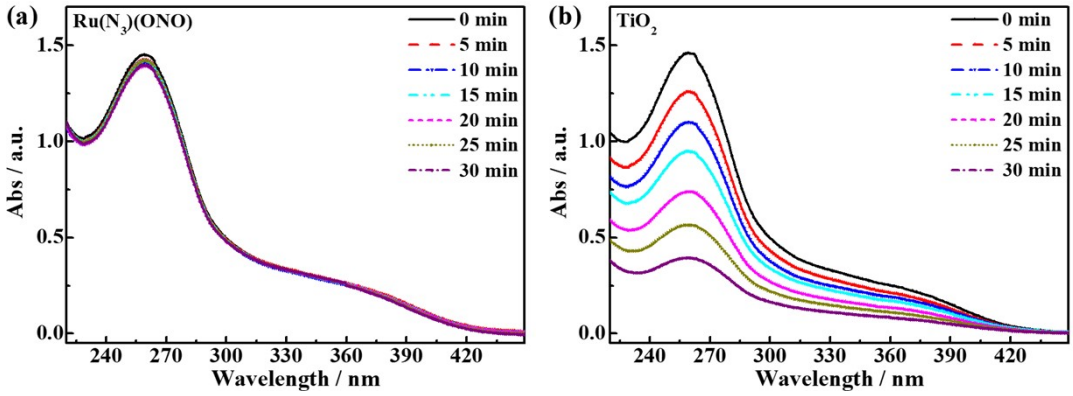

Fig. S11 UV-Vis absorption spectra of the NBT solution containing $Ru(N_3)(ONO)$ complex (a) or TiO_2 NPs (b) in dark or under Xe-lamp irradiation.

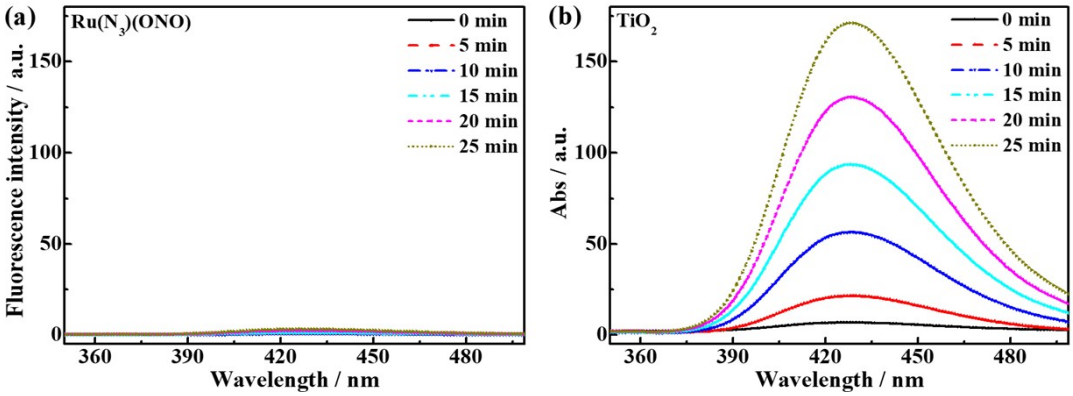

Fig. S12 Fluorescence spectra of the TA solution containing $Ru(N_3)(ONO)$ complex (a) or TiO_2 NPs (b) in dark or under Xe-lamp irradiation.

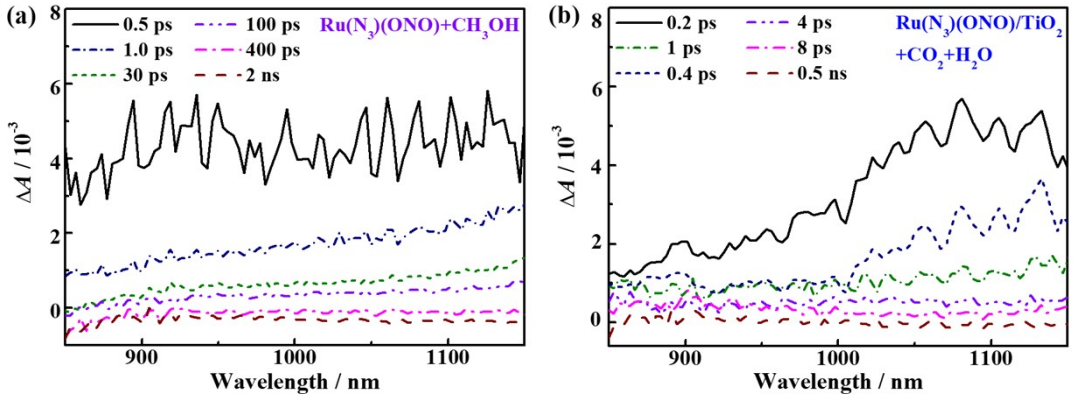

Fig. S13 The fs-TA spectra in NIR region of (a) $Ru(N_3)(ONO)$ in $MeCN:CH_3OH$ (95:5) purged with Ar gas for 15 min and (b) 0.25wt%$Ru(N_3)(ONO)/TiO_2$ in $MeCN:H_2O$ (95:5) purged with CO_2 gas for 15 min. Excitation with 400 nm light (200 μW).

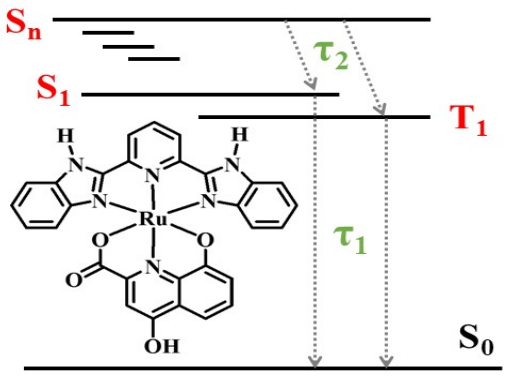

Fig. S14 Jablonski diagram for the photoinduced dynamics of $Ru(N_3)(ONO)$ complex in acetonitrile.